Molecular-state close-coupling theory including continuum states. II. Packet states and couplings for the proton–hydrogen-atom system

G. Bandarage and W. R. Thorson
Department of Chemistry, The University of Alberta, Edmonton, Alberta, Canada T6G 2G2
(Received 10 April 1987; revised manuscript received 8 September 1987)

The preceding paper (I) of this series develops a molecular-state close-coupling theory of ion-atom collisions including the electronic continuum, which is described by packet states spanning it locally. The present paper describes results of computations applying this formulation to the prototype problem of impact ionization in proton–hydrogen-atom collisions, in particular, studies of the properties of the basis states and the nonadiabatic couplings among them. (1) We construct continuum eigenfunctions using a "quantal momentum" or phase-amplitude representation and use this to study construction and properties of continuum packet states, and we show how localization of packet states within a specified interaction region leads to specification of packet widths and/or energies. (2) We verify assumptions made in the derivations given in paper I about nonadiabatic couplings of continuum states, and report computations of coupling matrix elements needed to implement the theory for this system. Subsequent work will present close-coupling calculations using this data.

I. INTRODUCTION

The first paper in this series[1] formulates a theory of close-coupling in slow ion-atom collisions using molecular electronic states as the expansion basis and including the continuum, which is represented by a discretized set of *packet states* spanning it locally and constructed from the exact continuum states. Inclusion of the effects of *escape* by continuum electrons from the local region spanned by the close-coupled basis is an important feature of the theory. Although specific attention was restricted to a simple class of problems, in which a single dynamical electron is excited by collision from an initially bound state to other bound levels or to a continuum lying entirely above the bound levels, the assumptions needed to derive the close-coupled integral equations of Ref. 1 are actually fairly broad and the theory can be extended, with suitable modifications, to a larger class of model problems. The discussion in Ref. 1 was therefore presented in the most general terms compatible with basic assumptions, and specific applications to particular systems were not a primary concern.

The theory of Ref. 1 is *directly* applicable to the problem of collisional (impact) ionization in one-electron prototype systems, for which the required assumptions may be justified quite rigorously. In this and succeeding papers in this series, we apply the theory to ionization in slow proton–H-atom collisions as an example. The description of the continuum given here is a considerable advance over previous close-coupling studies of H^+-H(1*s*) collisions, which have either omitted the continuum entirely,[2–4] represented it by a limited basis of pseudostates,[5] or treated continuum couplings only by first-order perturbation methods.[6] This formulation (1) uses a much more complete continuum description, (2) treats effects of close-coupling between continuum and discrete states *and* among the continuum components, and (3) allows us to assess the escape effects. These points can be addressed separately. Reference 1 presents integro-differential equations which show the relation between a correct formulation and the (probability-conserving) differential equations of conventional close-coupling treatments [Ref. 1, Eqs. (4.21) and (4.22)]; neglect of escape terms in these equations reduces this formulation to the conventional ones. Such a simplified calculation would give information on the first two points, and the effects of escape may be included as a further step.

In this paper we present detailed computational results bearing on the properties and couplings of the continuum states for the H_2^+ system (and packet states constructed from them). Results illustrate points made in Ref. 1, but are also relevant to recent work on this particular system. Emphasis is given to the results (displayed in figures and tables) and derivations and descriptions of computational methods are kept to a minimum.[7]

Section II is concerned with construction and properties of the continuum packet states, following the scheme described in Sec. III of Ref. 1. We find that these have densities concentrated mainly at the center of nuclear charge of the molecular system, even for large internuclear separations, i.e., they remain localized on the center of charge and do not follow the individual nuclei. We have computed tables of packet energy widths appropriate to basis sets spanning the continuum within localized regions of specified size.

Section III is concerned with the properties of nonadiabatic couplings among continuum states. We examine their behavior for H_2^+, especially in relation to the singularities exhibited when the coupled states are degenerate, using the generalized Hellmann-Feynman relations derived in Ref. 1. Results show that the assumptions made in deriving the coupled integral equations of Ref. 1 are indeed valid for this prototype system. Subse-

quent work will carry out close-coupling calculations using results outlined here.

II. CONTINUUM PACKET STATES

A. Phase-amplitude description of continuum states

Exact continuum states for the H_2^+ system are the eigenfunctions $\phi(\epsilon\mu\lambda;\mathbf{r};\mathbf{R})$ of the electronic Hamiltonian $H_e(\mathbf{r};\mathbf{R})$ at each nuclear configuration $\mathbf{R}$,

$$H_e(\mathbf{r};\mathbf{R})\phi(\epsilon\mu\lambda;\mathbf{r};\mathbf{R})=\epsilon\phi(\epsilon\mu\lambda;\mathbf{r};\mathbf{R}) \ . \tag{2.1}$$

They are separable in prolate spheroidal coordinates $[(\xi,\eta,\varphi),\ 1\le\xi<\infty,\ -1\le\eta\le+1,\ 0\le\varphi<2\pi]$,

$$\phi(\epsilon\mu\lambda;\mathbf{r};\mathbf{R})=X(\epsilon\mu\lambda;\xi;R)S(\epsilon\mu\lambda;\eta;R)e^{i\lambda\varphi}/\sqrt{2\pi} \ ,$$

and $X(\epsilon\mu\lambda;\xi;R)$ and $S(\epsilon\mu\lambda;\eta;R)e^{i\lambda\varphi}/\sqrt{2\pi}$ are called *radial* and *angular* wave functions, respectively. λ is the component of orbital angular momentum on the molecular axis, and the index μ labels the separation constant $A_{\mu\lambda}$, which may be computed as the (discrete) eigenvalue of the angular equation for given energy ϵ and configuration R; in the united-atom limit $R\to0$, $A_{\mu\lambda}$ specifies the total angular momentum,

$$A_{\mu\lambda}\to\mu(\mu+1),\quad \mu=|\lambda|,\quad |\lambda|+1,\quad \text{etc} \ .$$

Continuum wave functions for the one-electron two-center system have been computed previously by several workers,[8–12] but here we found it computationally and conceptually more useful to develop a new representation of the radial wave functions in the *quantal momentum* or phase-amplitude form,[13–18]

$$X(\epsilon\mu\lambda;\xi;R)=2/[\pi R(\xi^2-1)]^{1/2}[p_r(\epsilon\mu\lambda;\xi;R)]^{-1/2} \times\sin\theta(\epsilon\mu\lambda;\xi;R) \ , \tag{2.2a}$$

where the *phase* $\theta(\epsilon\mu\lambda;\xi;R)$ defined by

$$\theta(\epsilon\mu\lambda;\xi;R)\equiv\int_1^{\xi}d\xi' p_r(\epsilon\mu\lambda;\xi';R) \tag{2.2b}$$

and the *quantal momentum* $p_r(\epsilon\mu\lambda;\xi;R)$ are easily computed, slowly varying functions of their arguments. These functions are computed as follows: The substitution $X(\xi)=F(\xi)/(\xi^2-1)^{1/2}$ in the radial equation gives

$$F''(\xi)+P_c^2(\xi)F(\xi)=0 \ , \tag{2.3a}$$

where

$$\begin{aligned}P_c^2(\xi)&\equiv c^2+(q\xi-A_{\mu\lambda}+c^2)/(\xi^2-1)\\&\quad-(\lambda^2-1)/(\xi^2-1)^2 \ ,\\ c^2&=\epsilon R^2/2,\quad q=(Z_A+Z_B)R\end{aligned} \tag{2.3b}$$

(nuclear charges Z_A,Z_B), and we seek the solution F_s regular at the origin $\xi=1$. A fundamental solution pair is written in the form

$$f_{\pm}(\xi)=\exp\left[\pm i\int^{\xi}d\xi' p_{\pm}(\xi')\right]$$

and then $p_{\pm}(\xi)$ satisfies the equations

$$\mp ip'_{\pm}(\xi)+p_{\pm}^2(\xi)=P_c^2(\xi) \tag{2.4a}$$

and depends on a single *real* function $p_r(\xi)$,

$$p_{\pm}(\xi)=p_r(\xi)\pm i[p_r'(\xi)/2p_r(\xi)] \ . \tag{2.4b}$$

The *quantal momentum* is uniquely defined as that solution of Eqs. (2.4) satisfying the asymptotic boundary condition

$$p_r(\xi)\to P_c(\xi),\quad \xi\to\infty \ .$$

Global solutions for $p_r(\xi)$ and $\theta(\xi)$ are generated by (1) initiating solutions by a suitable asymptotic approximation at large ξ, (2) numerically integrating Eqs. (2.4) and the phase integral inward toward $\xi=1$ and, at a point ξ_0 suitably near the origin, (3) matching regular and irregular trigonometric solutions of the forms

$$F_s(\xi)\equiv[p_r(\xi)]^{-1/2}\sin\theta(\xi) \ ,$$

$$F_c(\xi)\equiv[p_r(\xi)]^{-1/2}\cos\theta(\xi)$$

[where $\theta(\xi)$ is defined by Eq. (2.2b)] to linear combinations of regular and irregular power-series solutions of Eq. (2.2a) about $\xi=1$. A more detailed description of the computational method is given elsewhere.[7]

$p_r(\xi)$ and $\theta(\xi)$ have the asymptotic forms

$$p_r(\epsilon\mu\lambda;\xi;R)\simeq c+(q/2c)/\xi+O(\xi^{-2}) \ , \tag{2.5a}$$

$$\theta(\epsilon\mu\lambda;\xi;R)\simeq c\xi+(q/2c)\ln(c\xi)+\delta(\epsilon\mu\lambda;R)+O(\xi^{-1}) \ , \tag{2.5b}$$

where $\delta(\epsilon\mu\lambda;R)$ is the phase shift.

More efficient generation and storage of the continuum wave functions are possible in this form because the quantal momentum and phase functions are slowly varying, nonoscillatory functions of ξ over essentially the entire domain $1\le\xi<\infty$. They are also slowly varying functions of the parameters ϵ and R, a fact we use in computing packet-state properties.

Figures 1 and 2 show some typical plots of quantal momentum and phase for a number of continuum states of H_2^+. Also shown for comparison are suitable JWKB approximations to these variables.

B. Packet states

We define continuum packet states $\tilde{\phi}(j\mu\lambda;\mathbf{r};\mathbf{R})$ as superpositions of the exact continuum states with uniform amplitudes over a packet width Δ_j centered on a mean energy ϵ_j,

$$\tilde{\phi}(j\mu\lambda;\mathbf{r};\mathbf{R})\equiv(\Delta_j)^{-1/2}\int_{\epsilon_j-\Delta_j/2}^{\epsilon_j+\Delta_j/2}d\epsilon\,\phi(\epsilon\mu\lambda;\mathbf{r};\mathbf{R}) \ , \tag{2.6a}$$

where

$$\epsilon_{j+1}=\epsilon_j+(\Delta_j+\Delta_{j+1})/2,\quad j=1,2,\ldots,\quad \epsilon_1=\Delta_1/2 \ , \tag{2.6b}$$

and the *packet widths* Δ_j are not yet defined. We showed in Ref. 1 that the packet states are localized in a region near the nuclei,

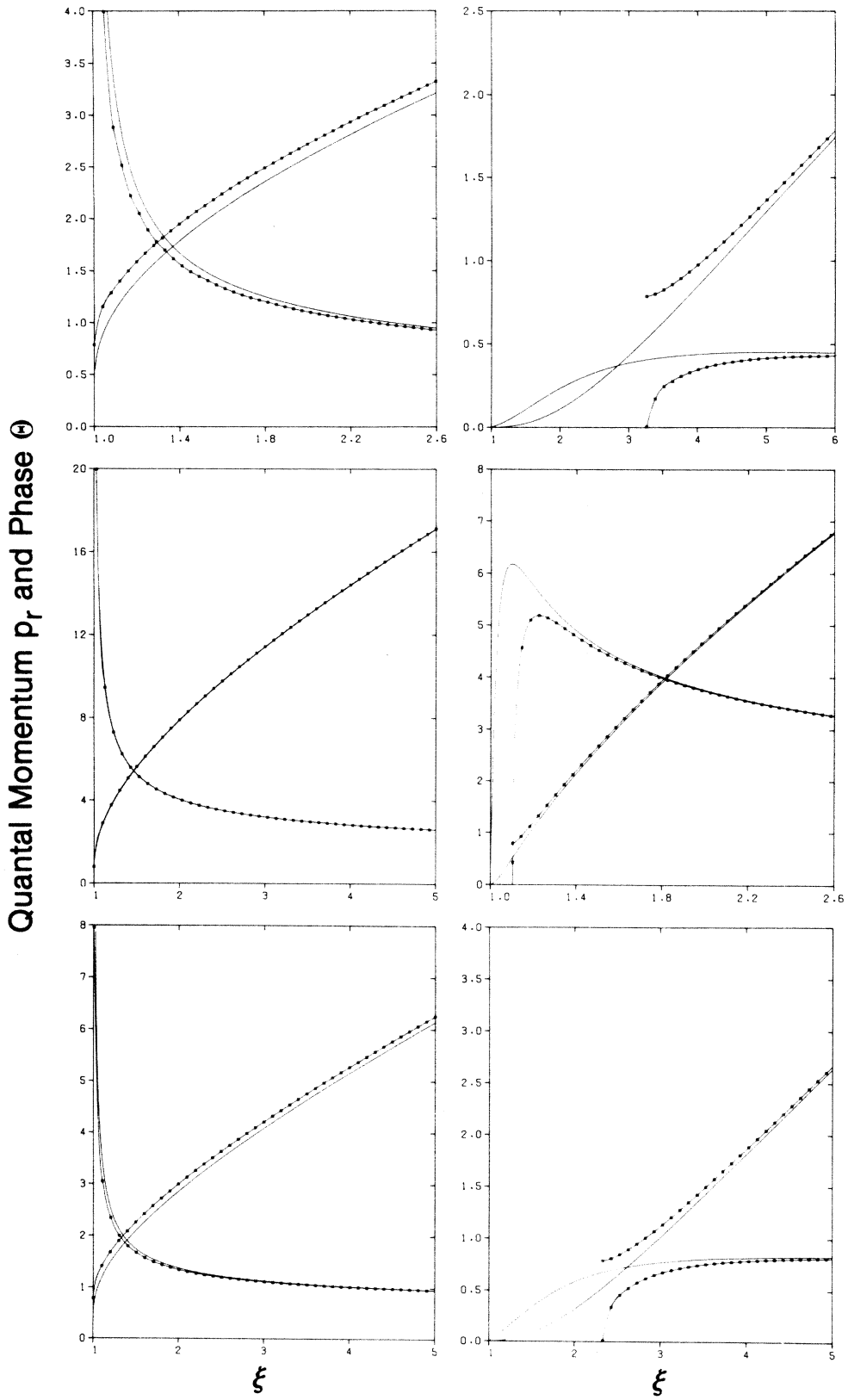

FIG. 1. Quantal momentum and phase vs ξ (solid curves) for quantum numbers (μ,λ), internuclear distance R (a.u.), and continuum energy ϵ (a.u.). Curves with attached data points show the corresponding JWKB approximations. Left-hand figures, top to bottom, are for $(\mu,\lambda)=(0,0)$ and (a) $R=1.0$, $\epsilon=0.05$; (b) $R=10.0$, $\epsilon=0.05$; (c) $R=1.0$, $\epsilon=1.00$. Right-hand figures show same R,ϵ values for $(\mu,\lambda)=(2,2)$.

$$\tilde{\phi}(j\mu\lambda;\mathbf{r};\mathbf{R}) \simeq \Delta_j^{1/2}\phi(\epsilon_j\mu\lambda;\mathbf{r};\mathbf{R}) f(\Delta_j(\partial\theta/\partial\epsilon)_{\epsilon_j}/2) , \tag{2.7}$$

where $f(x)=x^{-1}\sin x$; since $(\partial\theta(\epsilon\mu\lambda;\xi;R)/\partial\epsilon)_{\epsilon_j}$ is a uniformly increasing function of ξ, f is a *packet envelope function* whose magnitude decreases strongly for $\xi > \xi_d$ such that

$$\Delta_j[\partial\theta(\epsilon\mu\lambda;\xi_d;R)/\partial\epsilon]_{\epsilon_j} = 2\pi . \tag{2.8}$$

Hence the width Δ_j determines the spatial localization of the packet state $\tilde{\phi}(j\mu\lambda;\mathbf{r};\mathbf{R})$.

Define a prolate spheroidal interaction region with a fixed *major radius* r_d, which specifies $\xi_d = 2r_d/R$ for a given internuclear distance R. Then for a given set of quantum numbers (μ,λ), Eqs. (2.6b) and (2.8) jointly specify a consistent set of packet widths $\{\Delta_j\}$ such that the corresponding packet states $\{\tilde{\phi}(j\mu\lambda;\mathbf{r};\mathbf{R})\}$ are all localized within this region, according to Eq. (2.7). However, two practical questions arise: (1) The formalism of Ref. 1 assumes the widths $\{\Delta_j\}$ are independent of internuclear distance R (and hence independent of time). Is the above specification consistent with this? (2) Are the widths $\{\Delta_j\}$ independent of the quantum numbers (μ,λ)? We computed *packet width functions* defined by

$$\Delta(\mu\lambda;R;r_d;\epsilon) \equiv 2\pi/[\partial\theta(\epsilon\mu\lambda;\xi_d;R)/\partial\epsilon] \tag{2.9}$$

and examined their dependence on R and on (μ,λ) for various choices of major radius r_d. The results are fairly insensitive to the quantum numbers (μ,λ). The dependence on R is stronger for increasing $(\mu-\lambda)$ and decreasing energy ϵ and r_d, but there is a large domain

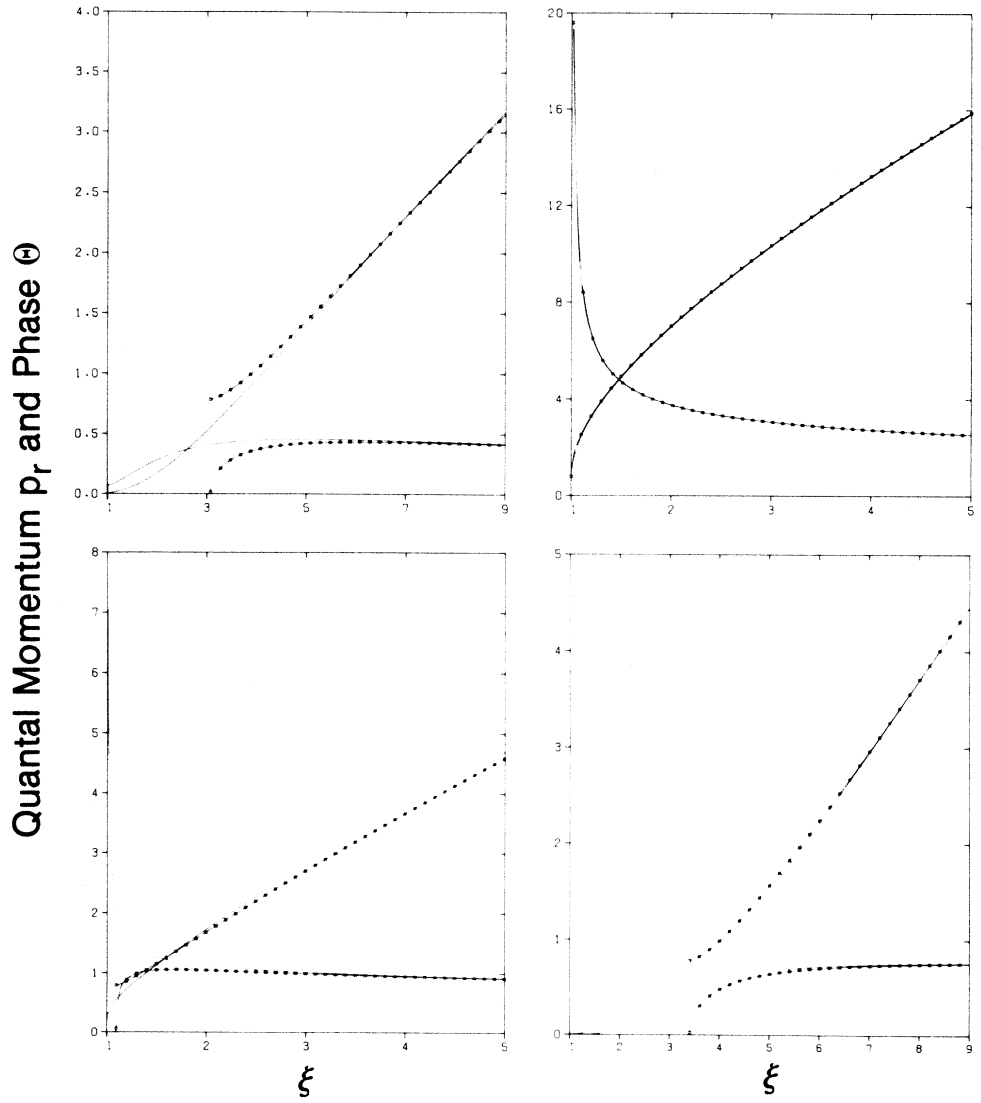

FIG. 2. Quantal momentum and phase vs ξ (solid curves) for quantum numbers (μ,λ), internuclear distance R (a.u.), and continuum energy ϵ (a.u.). Curves with attached data points show the corresponding JWKB approximations. Top figures from left are for $(\mu,\lambda)=(2,0)$, $\epsilon=0.05$, and $R=1.0$ and 10.0, respectively; bottom figures, $(\mu,\lambda)=(1,0)$, $R=1.0$, $\epsilon=1.00$ and $(\mu,\lambda)=(3,0)$, $R=1.0$, $\epsilon=1.00$.

over which this dependence is very small. In particular, for $r_d \geq 40.0$ a.u., $\epsilon \geq 0.05$ a.u., and $R \leq 20.0$ a.u., the maximum deviation of any function $\Delta(\mu\lambda;R;r_d;\epsilon)$ from the average for all states with $\mu \leq 2$ is less than 0.01 a.u. (10%); hence, to good approximation one can define a common packet width function independent of both R and (μ,λ). Figures 3 and 4 show the dependence of this function on energy ϵ and radius r_d. Using the packet width function for a given r_d, the packet widths and energies for an entire basis set of packet states localized in the corresponding "interaction region" are fixed by Eq. (2.6b). Tables of packet widths and energies are given in Table I for $r_d = 40.0$, 60.0, and 80.0 a.u. Finally, Fig. 5 shows how the energy of the lowest packet, ϵ_1, varies with region size r_d.

To verify properties deduced above, we have constructed packet-state wave functions in the Cartesian (x,z) plane by explicit evaluation of the integrals (2.6a), using packet widths given in Table I. Quadratures with seven and nine points achieve convergence of the resulting amplitude functions at major maxima within 1×10^{-5} absolute error. Some typical plots resulting are shown in Fig. 6. Each picture represents a grid size 80×80 a.u. The decaying envelope is evident and though the graphs shown do not go out far enough to show the full decay we have verified by computation at selected further points that the predictions of Eq. (2.7) are valid.

The packet states display significant properties of the molecular continuum. For moderate values of the quantum numbers (μ,λ) the packet-state densities are centered not on the nuclei but on the center of positive charge and *remain* there as internuclear distance R increases. Densities located near the nuclei can be maintained only by continually increasing the quantum numbers (μ,λ) as R increases. Hence (a) molecular continuum packet states are *not* linear combinations of the atomic continuum packet states [i.e., not "LCAO"-like (where LCAO represents linear combination of atomic orbitals)] and (b) the molecular packet-state basis, if restricted to only the lowest 10 (μ,λ), is essentially independent of and nonoverlapping with atomic packet states for all except small internuclear distances (say, $R \leq 2.5$–4.0 a.u.). These properties hold for both low and high electron energies ϵ.

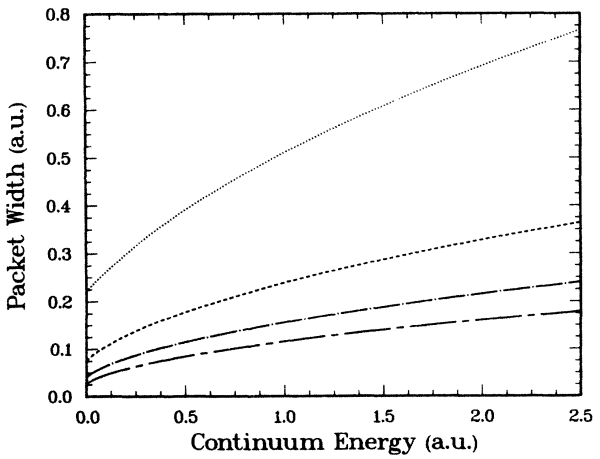

FIG. 3. Typical packet width function Δ vs continuum energy ϵ for several values of region size r_d [actual curves shown are for $(\mu,\lambda)=(0,0)$, $R=12.0$ a.u.]: $\cdots$, $r_d=20.0$ a.u.; ----, $r_d=40.0$ a.u.; -·-·-·-, $r_d=60.0$ a.u.; -----, $r_d=80.0$ a.u.

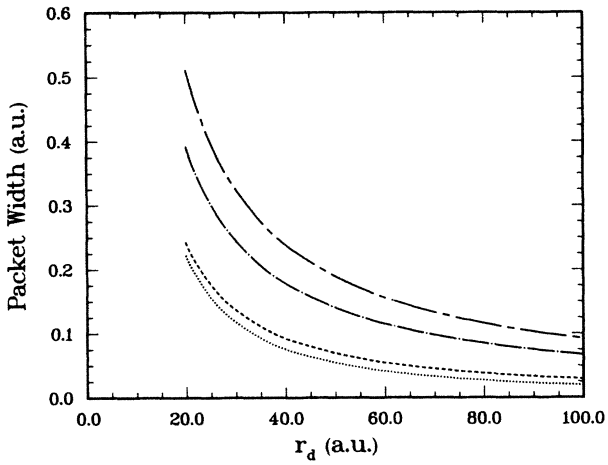

FIG. 4. Packet width function Δ vs region size r_d for several continuum energies ϵ [curves shown are for $(\mu,\lambda)=(0,0)$, $R=12.0$ a.u.]: $\cdots$, $\epsilon=0.001$ a.u.; ----, $\epsilon=0.05$ a.u.; -·-·-·-, $\epsilon=0.5$ a.u.; -----, $\epsilon=1.0$ a.u.

A recent close-coupling study by Winter and Lin[5] using a "triple-center" basis of pseudostates to represent the continuum indicated that ionization occurs predominantly to regions of configuration space centered at the "zero-force point," i.e., the molecular center of charge in this case, and they argued that this is an instance of the "Wannier mechanism" for three Coulomb particles. A quite different study by Olson,[19] based on Monte Carlo sampling of classical trajectories for the electron system, reached the same qualitative conclusion, that the ionized electron is located predominantly near the center of charge, and Olson recommends that basis sets having densities there be used for close-coupling studies of ionization. From the present work it is evident that the molecular continuum packet states have the appropriate spatial distribution properties and that these properties result from the geometry and fairly minimal mechanical assumptions, i.e., that if ionization occurs without imparting significant orbital angular momentum to the electron the resulting density will be centered at the center of positive charge rather than on the nuclei.

We can make some assessment of the adequacy of the packet-state basis for representing the molecular continuum within the specified interaction region. We find that the number of radial nodes between the origin and the interaction region boundary at ξ_d increases uniformly by 2 from a packet state with energy ϵ_j to the next higher one with energy ϵ_{j+1}. We think this argues favorably for the local completeness of the basis set.

TABLE I. Packet widths and energies for three values of interaction region size parameter r_d (all quantities in a.u.).

	$r_d=40.0$			$r_d=60.0$			$r_d=80.0$	
j	ϵ_j	Δ_j	j	ϵ_j	Δ_j	j	ϵ_j	Δ_j
1	0.0450	0.0900	1	0.0250	0.0500	1	0.0150	0.0300
2	0.1500	0.1200	2	0.0800	0.0600	2	0.0500	0.0400
3	0.2825	0.1450	3	0.1450	0.0700	3	0.0925	0.0450
4	0.4400	0.1700	4	0.2200	0.0800	4	0.1400	0.0500
5	0.6200	0.1900	5	0.3075	0.0950	5	0.1950	0.0600
6	0.8250	0.2200	6	0.4075	0.1050	6	0.2575	0.0650
7	1.0600	0.2500	7	0.5175	0.1150	7	0.3250	0.0700
8	1.3225	0.2750	8	0.6400	0.1300	8	0.3975	0.0750
9	1.6100	0.3000	9	0.7750	0.1400	9	0.4775	0.0850
10	1.9225	0.3250	10	0.9200	0.1500	10	0.5650	0.0900
11	2.2600	0.3500	11	1.0750	0.1600	11	0.6575	0.0950
			12	1.2400	0.1700	12	0.7550	0.1000
			13	1.4175	0.1850	13	0.8600	0.1100
			14	1.6075	0.1950	14	0.9725	0.1150
			15	1.8075	0.2050	15	1.0900	0.1200
			16	2.0175	0.2150	16	1.2125	0.1250
			17	2.2375	0.2250	17	1.3425	0.1350
						18	1.4800	0.1400
						19	1.6225	0.1450
						20	1.7700	0.1500
						21	1.9250	0.1600
						22	2.0875	0.1650
						23	2.2550	0.1700

III. COUPLING MATRIX ELEMENTS

As shown in Ref. 1, the Hellmann-Feynman theorem may be extended for the calculation of nonadiabatic couplings among continuum states of the one-electron prototype systems. For *radial couplings,* the matrix elements coupling two states, $\phi(\epsilon\mu\lambda;\mathbf{r};\mathbf{R})$ and $\phi(\epsilon'\mu'\lambda;\mathbf{r};\mathbf{R})$, have the form

$$\langle\phi(\epsilon'\mu'\lambda;\mathbf{R})\,|\,(\partial/\partial R)_r\,|\,\phi(\epsilon\mu\lambda;\mathbf{R})\rangle = \langle\epsilon\mu'\lambda;\mathbf{R}\,|\,\mathcal{D}^R\,|\,\epsilon\mu\lambda;\mathbf{R}\rangle\delta(\epsilon'-\epsilon) + \mathcal{P}\left[\frac{\langle\epsilon'\mu'\lambda;\mathbf{R}\,|\,(\partial H_e/\partial R)_r\,|\,\epsilon\mu\lambda;\mathbf{R}\rangle}{\epsilon-\epsilon'}\right], \quad (3.1)$$

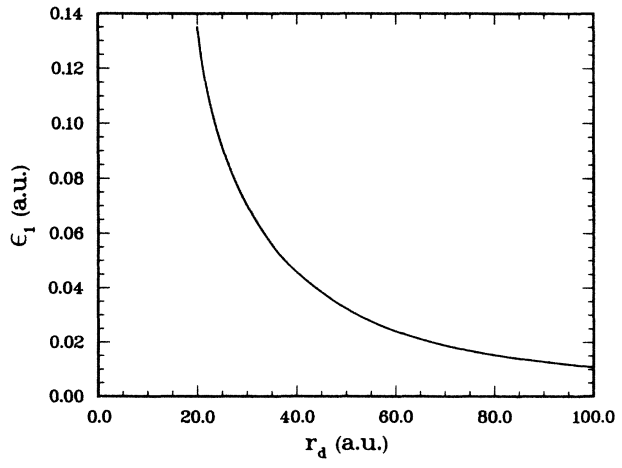

FIG. 5. Energy ϵ_1 of lowest packet state vs interaction region size parameter r_d.

where $\mathcal{P}$ means a principal value is taken in integrations over continuum energies. It was shown (cf. Appendix 1, Ref. 1) that the analytic coefficient of the singular term in Eqs. (3.1) is given by

$$\langle\epsilon\mu'\lambda;\mathbf{R}\,|\,\mathcal{D}^R\,|\,\epsilon\mu\lambda;\mathbf{R}\rangle=(1-\delta_{\mu'\mu})\mathcal{S}^R_{\mu'\mu}\cos\Delta^R_{\mu'\mu}\,, \quad (3.2a)$$

where

$$\Delta^R_{\mu'\mu}=\delta(\epsilon\mu'\lambda;R)-\delta(\epsilon\mu\lambda;R) \quad (3.2b)$$

and

$$\mathcal{S}^R_{\mu'\mu}=\int_{-1}^{1}d\eta\,S(\epsilon\mu'\lambda;\eta;R)[\partial S(\epsilon\mu\lambda;\eta;R)/\partial R]_\eta = [\epsilon R/(A_{\mu'\lambda}-A_{\mu\lambda})]\int_{-1}^{1}d\eta\,S(\epsilon\mu'\lambda;\eta;R)\times\eta^2 S(\epsilon\mu\lambda;\eta;R)\,, \quad (3.2c)$$

and also that when $\epsilon'=\epsilon$ the commutator matrix element in Eq. (3.1) reduces to

$$\langle\epsilon\mu'\lambda;\mathbf{R}\,|\,(\partial H_e/\partial R)_r\,|\,\epsilon\mu\lambda;\mathbf{R}\rangle = (1/\pi)\{(1-\delta_{\mu'\mu})\mathcal{S}^R_{\mu'\mu}\sin\Delta^R_{\mu'\mu} - \delta_{\mu'\mu}[\partial\delta(\epsilon\mu\lambda;R)/\partial R]\}\,. \quad (3.2d)$$

Similarly, for the *angular couplings,*

$$\langle\epsilon'\mu'\lambda\pm1;\mathbf{R}\,|\,L_\pm\,|\,\epsilon\mu\lambda;\mathbf{R}\rangle = \langle\epsilon\mu'\lambda\pm1;\mathbf{R}\,|\,\mathcal{D}^\vartheta_\pm\,|\,\epsilon\mu\lambda;\mathbf{R}\rangle\delta(\epsilon'-\epsilon) + \mathcal{P}\left[\frac{\langle\epsilon'\mu'\lambda;\mathbf{R}\,|\,[L_\pm,H_e]\,|\,\epsilon\mu\lambda;\mathbf{R}\rangle}{\epsilon-\epsilon'}\right]; \quad (3.3)$$

the analytic coefficient of the singular term is

$$\langle \epsilon\mu'\lambda\pm 1;\mathbf{R} \mid \mathcal{D}^{\vartheta}_{\pm} \mid \epsilon\mu\lambda;\mathbf{R}\rangle = \mathcal{S}^{\pm}_{\mu'\mu}\cos\Delta^{\pm}_{\mu'\mu} , \tag{3.4a}$$

where

$$\Delta^{\pm}_{\mu'\mu} = \delta(\epsilon\mu'\lambda\pm 1;R) - \delta(\epsilon\mu\lambda;R) , \tag{3.4b}$$

$$\mathcal{S}^{\pm}_{\mu'\mu} = \int_{-1}^{1} d\eta\; S(\epsilon\mu'\lambda;\eta;R) L^{\eta}_{\pm} S(\epsilon\mu\lambda;\eta;R) , \tag{3.4c}$$

with

$$L^{\eta}_{\pm} = \mp(1-\eta^2)^{1/2}[(\partial/\partial\eta) \pm \lambda\eta/(1-\eta^2)] ,$$

and when $\epsilon' = \epsilon$ the commutator matrix element is

$$\langle \epsilon\mu'\lambda\pm 1;\mathbf{R} \mid [L_{\pm}, H_e] \mid \epsilon\mu\lambda;\mathbf{R}\rangle = (1/\pi)\mathcal{S}^{\pm}_{\mu'\mu}\sin\Delta^{\pm}_{\mu'\mu} . \tag{3.4d}$$

In Ref. 1 we showed that to form a valid representation of the nonadiabatic coupling operator within the truncated subspace spanned by the packet states one must take explicit account of any energy dependence in the couplings which varies rapidly over a packet width.

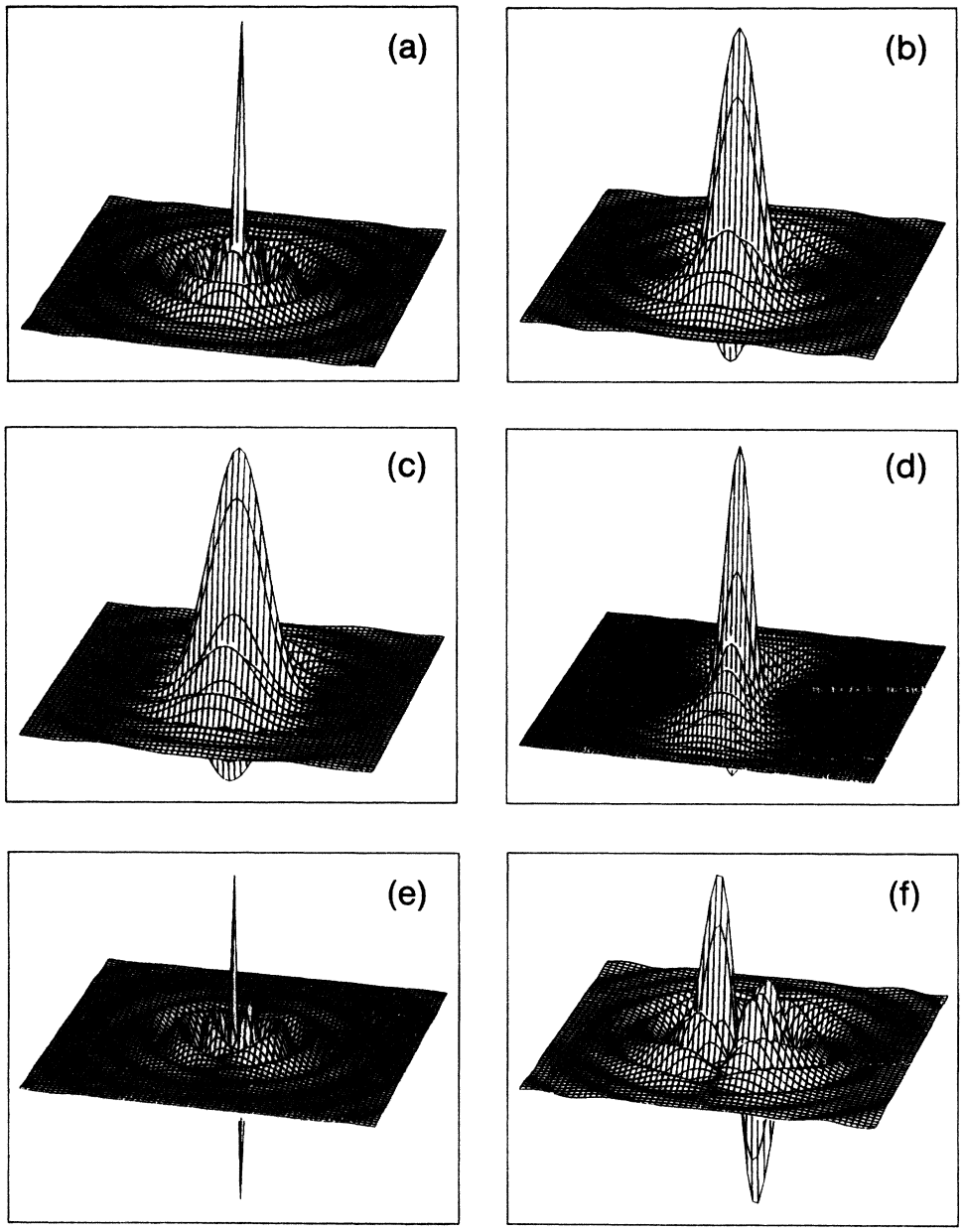

FIG. 6. Continuum packet states in the (x,z) plane, showing localization of packets at the center of charge. Interaction region size parameter $r_d = 40.0$ a.u.; each picture shows a region 80×80 a.u. (μ,λ) and (R,ϵ) values as follows: (a) $\mu=0$, $\lambda=0$, $R=2.0$ a.u., $\epsilon=0.150$ a.u.; (b) $\mu=0$, $\lambda=0$, $R=20.0$ a.u., $\epsilon=0.150$ a.u.; (c) $\mu=0$, $\lambda=0$, $R=40.0$ a.u., $\epsilon=0.150$ a.u.; (d) $\mu=0$, $\lambda=0$, $R=20.0$ a.u., $\epsilon=0.825$ a.u.; (e) $\mu=1$, $\lambda=0$, $R=2.0$ a.u., $\epsilon=0.150$ a.u.; (f) $\mu=1$, $\lambda=0$, $R=20.0$ a.u., $\epsilon=0.150$ a.u.; (g) $\mu=1$, $\lambda=0$, $R=40.0$ a.u., $\epsilon=0.150$ a.u.; (h) $\mu=1$, $\lambda=0$, $R=20.0$ a.u., $\epsilon=0.825$ a.u.; (i) $\mu=2$, $\lambda=1$, $R=2.0$ a.u., $\epsilon=0.150$ a.u.; (j) $\mu=2$, $\lambda=1$, $R=20.0$ a.u., $\epsilon=0.150$ a.u.; (k) $\mu=2$, $\lambda=1$, $R=40.0$ a.u., $\epsilon=0.150$ a.u.; (l) $\mu=2$, $\lambda=1$, $R=20.0$ a.u., $\epsilon=0.825$ a.u.

We used the structure given by the Hellmann-Feynman relations [Eqs. (3.1) and (3.3)] as an assumed general form for the couplings, and assumed that the analytic coefficients of the singular terms and the numerators in the principal-value terms are slowly varying functions of continuum energy over a packet width. This assumption is investigated here for the proton–H-atom system, and we find it is valid to a good approximation. Finally, we have computed the matrix elements needed in Eqs. (3.1) and (3.3) for energies ϵ',ϵ corresponding to packet energies ϵ_j given in Table I; using the formulas given in Ref. 1 for effective couplings of the packet states, these matrix elements provide data necessary for close-coupling calculations to follow in later work.

The quantities displayed in Figs. 7–10 are just the commutator matrix elements

$$\langle \epsilon'\mu'\lambda;R \mid \mathbf{P}^R \mid \epsilon\mu\lambda;R \rangle \equiv \langle \epsilon\mu'\lambda;R \mid (\partial H_e/\partial R)_r \mid \epsilon\mu\lambda;R \rangle , \tag{3.5a}$$

$$\langle \epsilon'\mu'\lambda\pm1;R \mid \mathbf{P}^{\vartheta} \mid \epsilon\mu\lambda;R \rangle \equiv \langle \epsilon\mu'\lambda\pm1;R \mid [L_+,H_e] \mid \epsilon\mu\lambda;R \rangle , \tag{3.5b}$$

appearing in Eqs. (3.1) and (3.3), and the quantities $\langle \epsilon\mu'\lambda;R \mid \mathcal{D}^R \mid \epsilon\mu\lambda;R \rangle$ and $\langle \epsilon\mu'\lambda\pm1;R \mid \mathcal{D}^{\vartheta}_+ \mid \epsilon\mu\lambda;R \rangle$ defined in Eqs. (3.2a) and (3.4a), respectively.

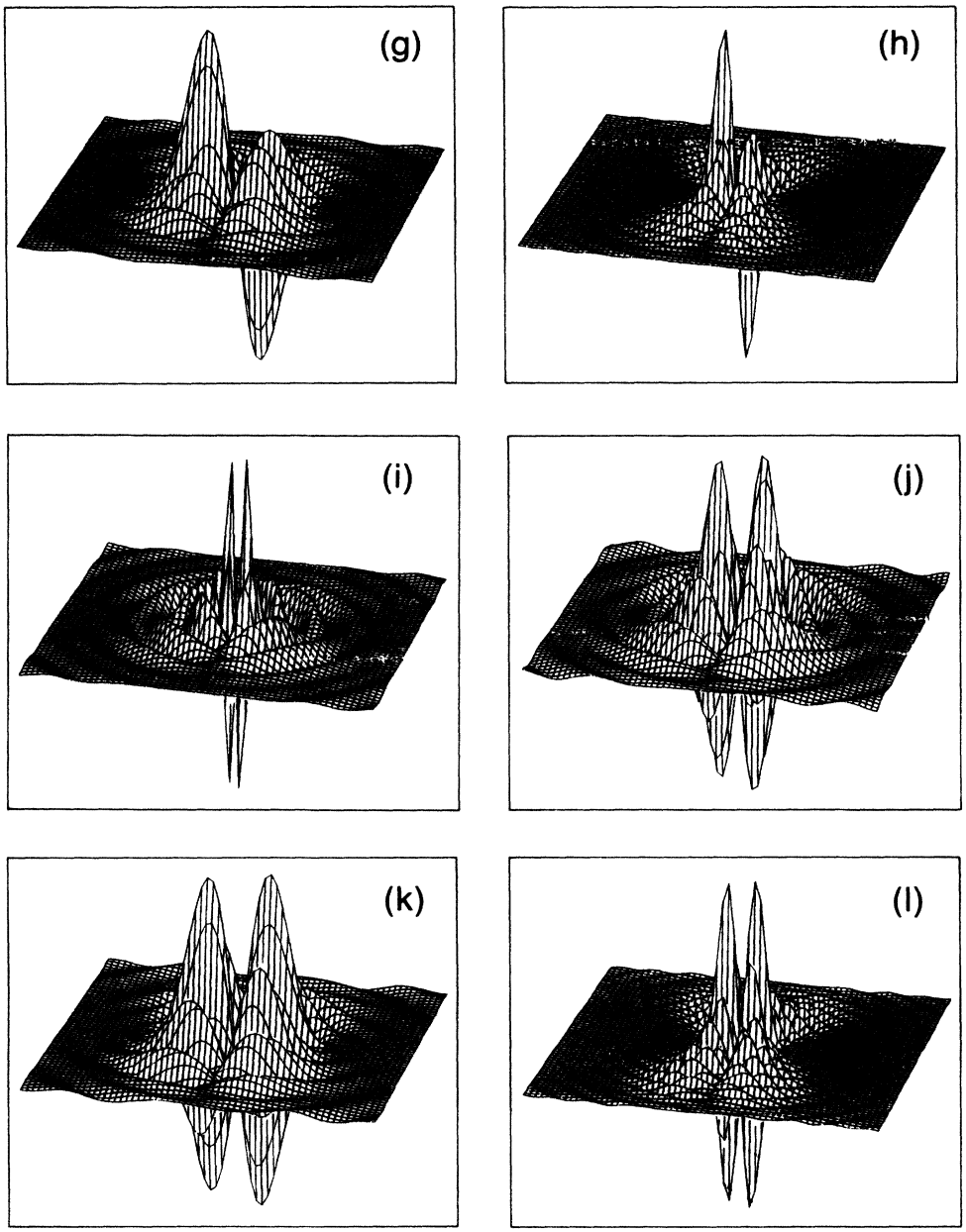

FIG. 6. (*Continued*).

Figures 7 and 8 display the dependence of the commutator matrix elements in Eqs. (3.5) upon continuum energies ϵ', ϵ. These are generally slowly varying over a packet width, though in a few cases the slopes are also significant, especially at large R; certainly, however, replacement by the mean value at the center of a packet is a reasonable first approximation. The qualitative behavior of the angular matrix elements (3.5b) does not depend much on the quantum numbers μ', μ, or λ, while in contrast, the radial matrix elements (3.5a) show a

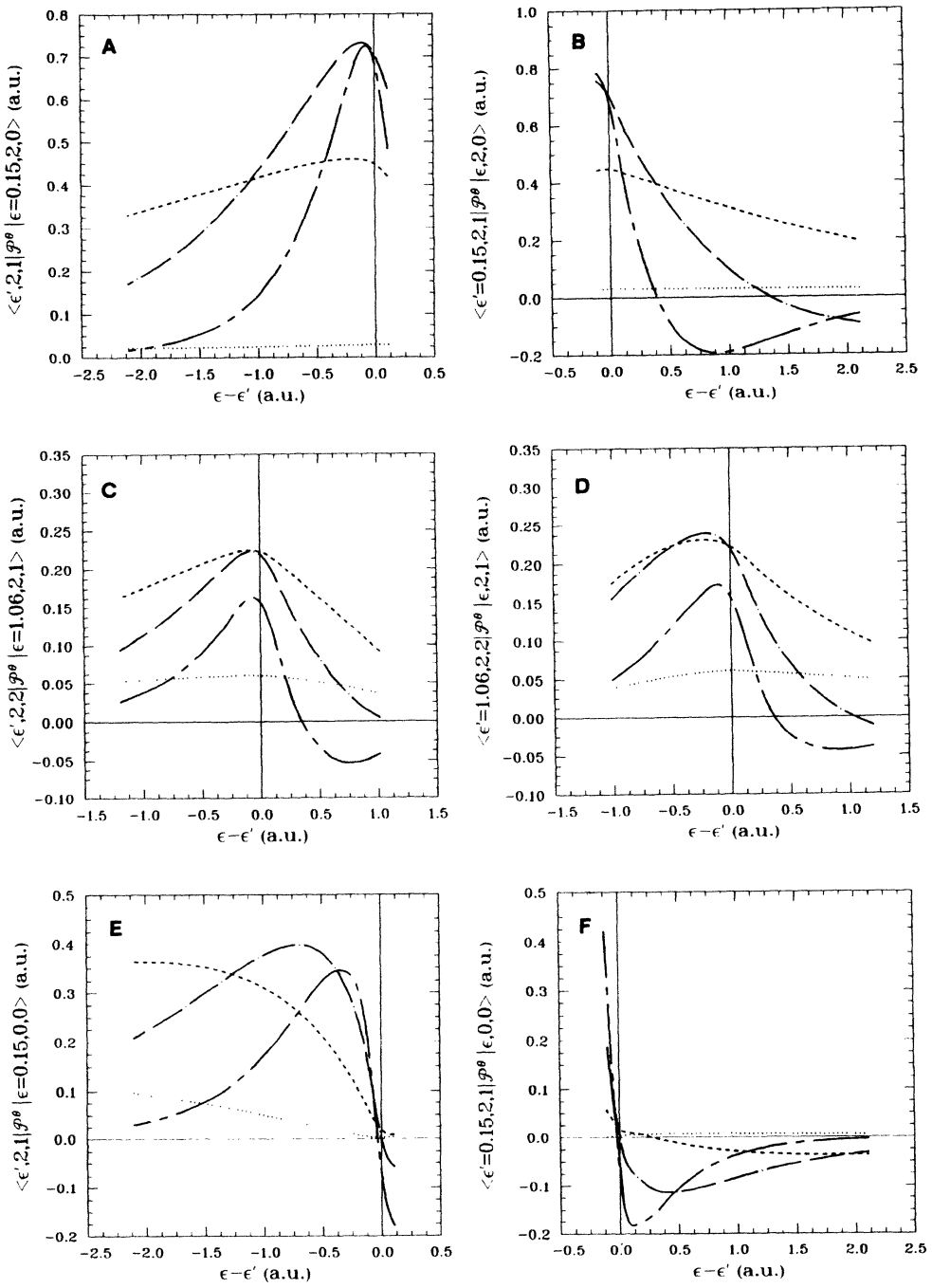

FIG. 7. Plots of angular matrix elements $\langle \epsilon'\mu'\lambda+1;R \mid \mathrm{P}^{\vartheta} \mid \epsilon\mu\lambda;R \rangle$ vs energy difference $(\epsilon-\epsilon')$ for several R values: $\cdots$, $R=1.0$ a.u.; ----, $R=3.0$ a.u.; -·-·-·-, $R=6.0$ a.u.; -----, $R=10.0$ a.u.

stronger dependence on these quantum numbers. In general, the magnitudes of both types of matrix elements decrease when one of the energies is large. The energy dependence of the δ-function coefficients is also shown in Fig. 8, and is generally much simpler.

In Figs. 9 and 10 the R dependence of the same matrix elements has been plotted for energies ϵ', ϵ corresponding to various packet-state energies ϵ_j in Table I. Again the behavior of the δ-function terms is simpler. In all cases the range of internuclear distances R over

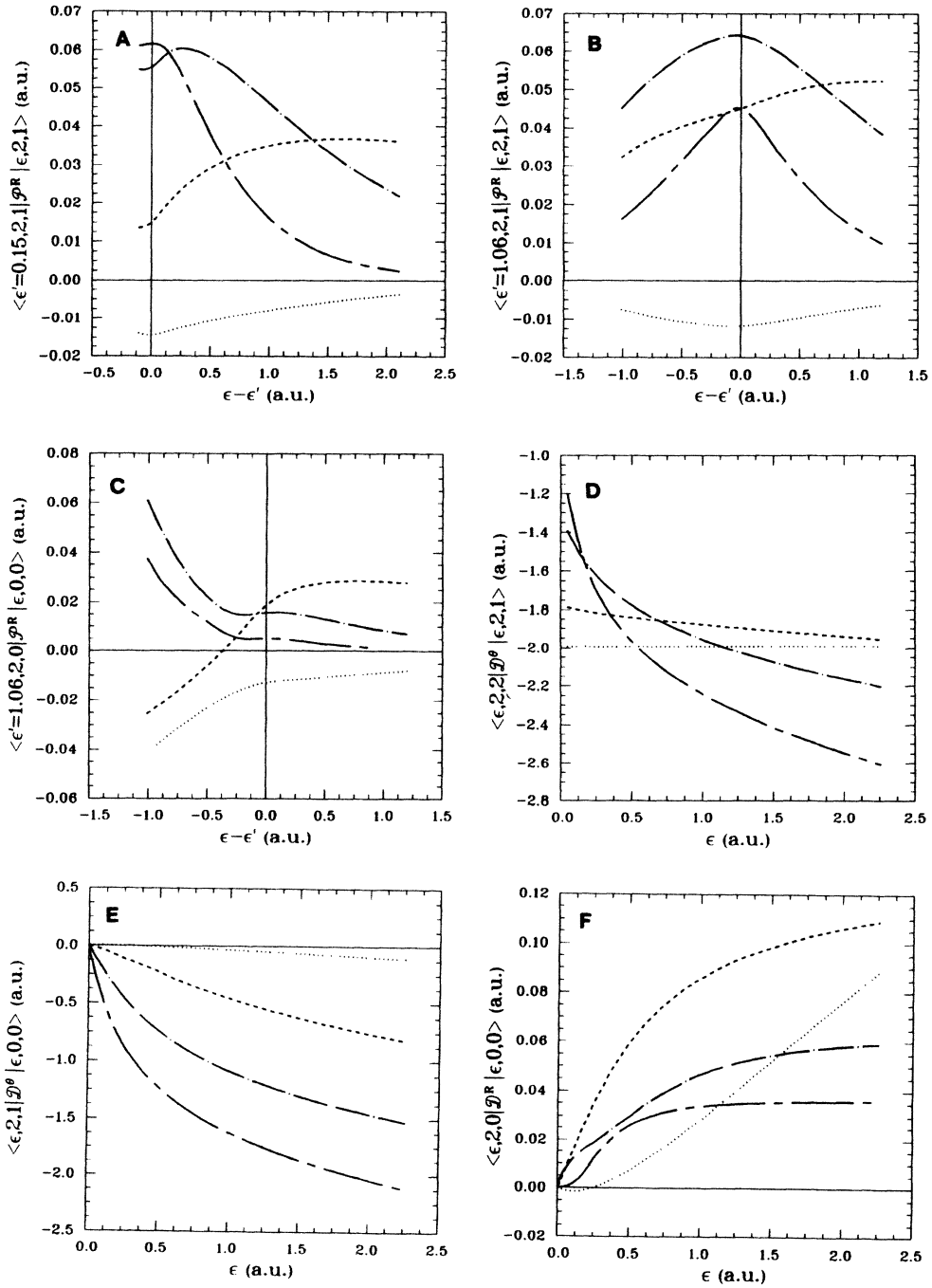

FIG. 8. Plots of radial matrix elements $\langle \epsilon'\mu'\lambda;R \mid P^R \mid \epsilon\mu\lambda;R \rangle$ vs energy difference $(\epsilon-\epsilon')$, and angular and radial δ-function coefficients $\langle \epsilon\mu'\lambda+1;R \mid \mathcal{D}^{\vartheta} \mid \epsilon\mu\lambda;R \rangle$, $\langle \epsilon\mu'\lambda;R \mid \mathcal{D}^{R} \mid \epsilon\mu\lambda;R \rangle$ vs energy ϵ, for several R values: ⋯, $R=1.0$ a.u.; – – – –, $R=3.0$ a.u.; –·–·–·–, $R=6.0$ a.u.; – – – –, $R=10.0$ a.u.

which the matrix elements are significant decreases as the energy difference increases. Note that for the angular coupling matrix elements an additional factor of R^{-1} must be included to get the true R dependence.

Ponomarev *et al.*[20] have reported calculations of some continuum-state nonadiabatic couplings relevant to the Coulomb three-body problem. The quantity these authors define as $Q_{ss'}^{(+)}$ [cf. their Eqs. (6) ff.] appears to be

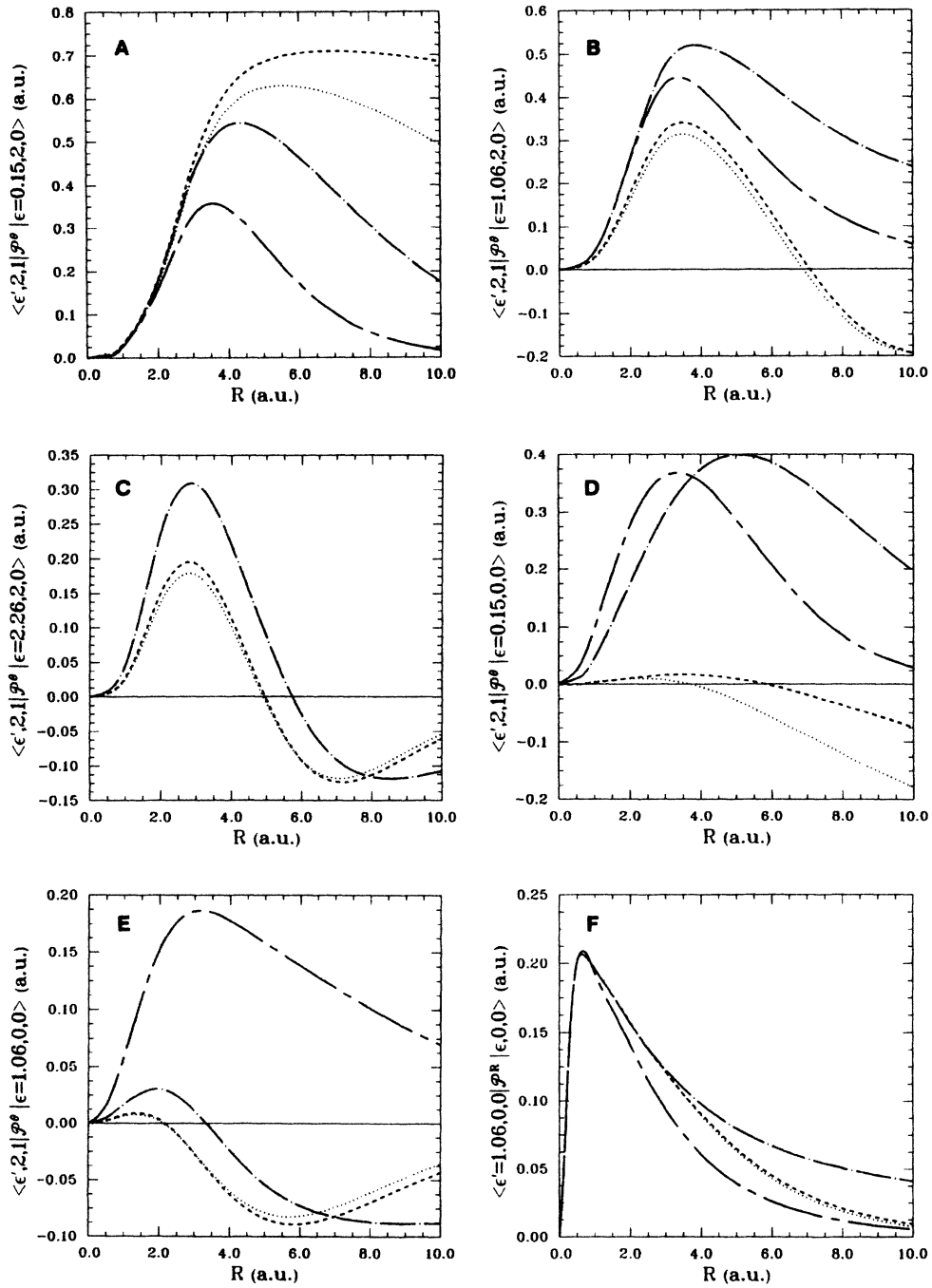

FIG. 9. Angular and radial matrix elements $\langle \epsilon'\mu'\lambda+1;R \mid \mathrm{P}^{\vartheta} \mid \epsilon\mu\lambda;R \rangle, \langle \epsilon'\mu'\lambda;R \mid \mathrm{P}^{R} \mid \epsilon\mu\lambda;R \rangle$ vs R for several energies ϵ: ⋯, $\epsilon=0.045$ a.u.; – – – –, $\epsilon=0.150$ a.u.; –·–·–·–, $\epsilon=1.06$ a.u.; – – – –, $\epsilon=2.26$ a.u.

the coefficient of the δ-function term in the radial coupling matrix element, given here by Eq. (3.2a). It is evident that their claim that this vanishes is *not* correct except when the two continuum states are the *same,* i.e., $\mu' = \mu$ (as is required from symmetry). They have not computed the principal-part matrix elements or the angular coupling matrix elements.

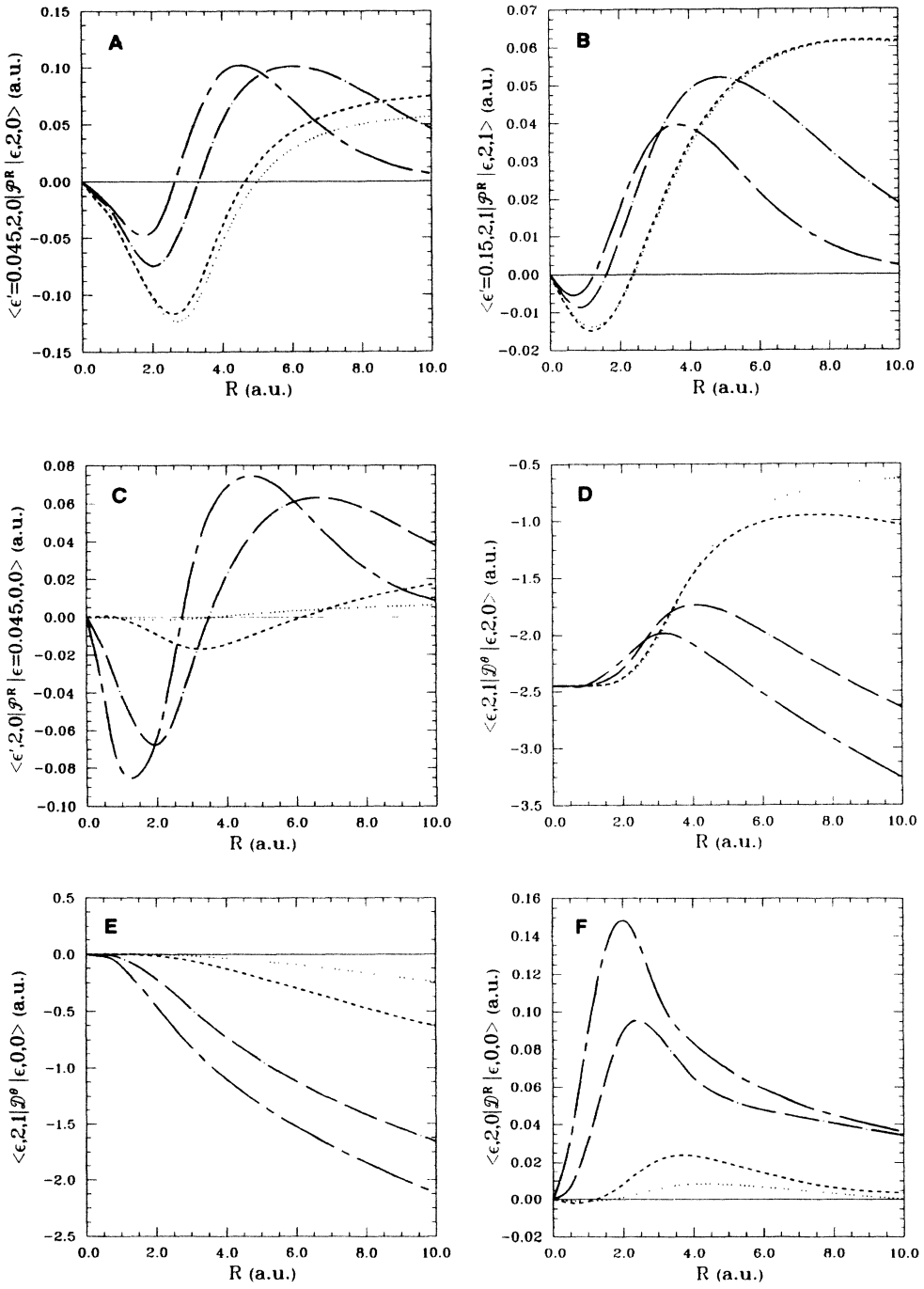

FIG. 10. Radial matrix elements $\langle \epsilon'\mu'\lambda; R \mid \mathrm{P}^R \mid \epsilon\mu\lambda; R \rangle$ and angular and radial δ-function coefficients $\langle \epsilon\mu'\lambda+1; R \mid \mathcal{D}^\vartheta \mid \epsilon\mu\lambda; R \rangle, \langle \epsilon\mu'\lambda; R \mid \mathcal{D}^R \mid \epsilon\mu\lambda; R \rangle$ vs R for several energies ϵ: ···, $\epsilon = 0.045$ a.u.; – – – –, $\epsilon = 0.150$ a.u.; –·–·–·–, $\epsilon = 1.06$ a.u.; – – – – –, $\epsilon = 2.26$ a.u.

ACKNOWLEDGMENTS

We thank the Natural Sciences and Engineering Research Council of Canada for support of this work through Operating Grant No. A-5330. One of us (G.B.) thanks the University of Alberta for partial support. Computations were performed on the Amdahl 5870 digital computer in the Department of Computing Services, University of Alberta.

[1]W. R. Thorson and G. Bandarage, Phys. Rev. A **37**, 692 (1988).
[2]M. Kimura and W. R. Thorson, Phys. Rev. A **24**, 1780 (1981).
[3]W. Fritsch and C. D. Lin, Phys. Rev. A **26**, 762 (1982).
[4]T. G. Winter and C. D. Lin, Phys. Rev. A **29**, 567 (1984).
[5]T. G. Winter and C. D. Lin, Phys. Rev. A **29**, 3071 (1984); **30**, 3323 (1984).
[6]V. SethuRaman, W. R. Thorson, and C. F. Lebeda, Phys. Rev. A **8**, 1316 (1973).
[7]More complete details of derivations and computations reported here may be found in a doctoral thesis presented by G. Bandarage in partial fulfillment of requirements for the Ph.D. degree, University of Alberta, 1987.
[8]G. Poots, U. Opik, and D. R. Bates, Proc. Phys. Soc. London, Sect. A **66**, 1113 (1953).
[9]H. Levy II and W. R. Thorson, Phys. Rev. **181**, 244 (1969).
[10]J. K. Cayford, W. R. Fimple, D. G. Unger, and S. P. White, J. Comput. Phys. **16**, 259 (1974).
[11]L. I. Ponomarev and L. N. Somov, J. Comput. Phys. **20**, 183 (1976).
[12]J. Rankin and W. R. Thorson, J. Comput. Phys. **32**, 437 (1979).
[13]W. E. Milne, Phys. Rev. **35**, 863 (1930); cf. also J. L. Powell and B. Crasemann, *Quantum Mechanics* (Addison-Wesley, Reading, MA, 1961), pp. 123–126.
[14]L. A. Young, Phys. Rev. **38**, 1612 (1931); **39**, 445 (1932).
[15]J. L. Peacher and J. G. Wills, J. Chem. Phys. **46**, 4809 (1967).
[16]W. I. Newman and W. R. Thorson, Can. J. Phys. **50**, 2997 (1972).
[17]J. C. Light and J. M. Yuan, J. Chem. Phys. **58**, 660 (1973); S. Y. Lee and J. C. Light, Chem. Phys. Lett. **25**, 435 (1974).
[18]H. J. Korsch and H. Laurent, J. Phys. B **14**, 4231 (1981); H. J. Korsch, H. Laurent, and R. Mohlenkamp, *ibid.* **15**, 1 (1982).
[19]R. E. Olson, Phys. Rev. A **33**, 4397 (1986).
[20]L. I. Ponomarev, S. Yu. Slavyanov, and L. N. Somov, J. Phys. B **13**, 3797 (1980).